Title

Anomalously Rapid Hydration Water Diffusion Dynamics Near DNA Surfaces

Journal

Journal of the American Chemical Society, 137(37)

ISSN

0002-7863

Authors

Franck, John M
Ding, Yuan
Stone, Katherine
et al.

Publication Date

2015-09-23

DOI

10.1021/jacs.5b05813

Peer reviewed

HHS Public Access

Author manuscript

J Am Chem Soc. Author manuscript; available in PMC 2016 September 23.

Published in final edited form as:

J Am Chem Soc. 2015 September 23; 137(37): 12013–12023. doi:10.1021/jacs.5b05813.

Anomalously rapid hydration water diffusion dynamics near DNA surfaces

John M. Franck[†,‡], **Yuan Ding**[¶], **Katherine Stone**[†,§], **Peter Z. Qin**[¶], and **Songi Han**[†]

Peter Z. Qin: pzq@usc.edu; Songi Han: songi@chem.ucsb.edu

[†]Department of Chemistry and Biochemistry, University of California, Santa Barbara, CA

[‡]National Biomedical Center for Advanced ESR Technology, Department of Chemistry and Chemical Biology, Cornell University, Ithaca, NY

[¶]Department of Chemistry, University of Southern California, Los Angeles, CA

[§]Pacira Pharmaceuticals, Inc, San Diego, CA

Abstract

The emerging Overhauser effect Dynamic Nuclear Polarization (ODNP) technique measures the translational mobility of water within the vicinity (5-15 Å) of preselected sites. The work presented here expands the capabilities of the ODNP technique and illuminates an important, previously unseen, property of the translational diffusion dynamics of water at the surface of DNA duplexes. We attach nitroxide radicals (*i.e.*, spin labels) to multiple phosphate backbone positions of DNA duplexes, allowing ODNP to measure the hydration dynamics at select positions along the DNA surface. With a novel approach to ODNP analysis, we isolate the contributions of water molecules at these sites that undergo free translational diffusion from water molecules that either loosely bind to or exchange protons with the DNA. The results reveal that a significant population of water in a localized volume adjacent to the DNA surface exhibits fast, bulk-like characteristics and moves unusually rapidly compared to water found in similar probe volumes near protein and membrane surfaces. Control studies show that the observation of these characteristics are upheld even when the DNA duplex is tethered to streptavidin or the mobility of the nitroxides is altered. This implies that, as compared to protein or lipid surfaces, it is an intrinsic feature of the DNA duplex surface that it interacts only weakly with a significant fraction of a network of surface hydration water. The displacement of this translationally mobile water is energetically less costly than that of more strongly bound water by up to several k_BT and thus can lower the activation barrier for interactions involving the DNA surface.

Introduction

The first few layers of water molecules that surround biomacromolecules typically exhibit distinctly different dynamics from those of bulk water,[1–3] and are termed “hydration water.” These hydration waters can modulate the activation barrier for molecular approach, yet are

Correspondence to: Peter Z. Qin, pzq@usc.edu; Songi Han, songi@chem.ucsb.edu.

Supporting Information **Available:** Further information on methodology, data analysis, and mathematical derivations. This material is available free of charge via the Internet at http://pubs.acs.org/.

extremely difficult to probe in the solution state. In particular, the nature of interactions between DNA and water remains an area of active exploration. Various methods have probed the dynamics of water at DNA surfaces. For example, ultrafast laser spectroscopy[4] senses the fluctuation of electric dipoles, while neutron scattering[5–7] senses the motion of hydrogen/deuterium nuclei, as averaged over the bulk sample, relying on relatively high concentrations of solute so that the hydration water can be observed. These studies have, in general, detected populations of relatively slow water dynamics on the surface of DNA. On the other hand, nuclear magnetic resonance (NMR) relaxation dispersion (NMRD) can sense the motion of a variety of nuclei and, when applied to DNA,[8] provides convincing evidence that the slowest moving water molecules are found in the minor groove and move with correlation times of only $\sim$ 200 ps. These NMRD studies conclude that any protons that surround DNA and exhibit motions at slower timescales, with correlation times of nanoseconds and slower, do so only because they are engaging in chemical exchange between the DNA and the nearby water molecules. Thus, one must consider the possibility that exchanging protons and water residing in the minor groove (on the $\sim$ 200 ps timescale) can potentially overwhelm the contribution from *other*, even faster moving hydration water, which is the subject of this study. In particular, this study focuses on ascertaining whether DNA is surrounded by a population of water molecules that translate on timescales of 3.5 – 5× slower than those in the bulk (and occasionally even slower timescales) – as is the case with proteins and lipids at room temperature [9–12] – or if the water molecules near DNA translate on a much faster timescale, close to that of the bulk.

While the release of tightly bound hydration waters can facilitate short-range, specific interactions, the fast-moving hydration waters that diffuse relatively freely across the hydration layer, with 1 – 3 times retardation relative to bulk water, might regulate the initial encounter between DNA and proteins at a longer range, as well as non-specific searches along DNA duplexes that are essential steps in protein/DNA recognition. Such fundamental properties of hydration water have been explored by a significant body of recent theoretical work, [13–17] which raises the possibility that the early stages of interactions between biomolecules can be regulated by enthalpic contributions from translationally mobile waters that constitute a dynamic network modulating the repulsive hydration barrier with varying magnitude.[18] By employing both molecular dynamics simulations and neutron scattering experiments, researchers have recently shown that the translational mobility of water couples intimately to the mobility of both structured and disordered proteins, and that the onset of translational mobility of the hydration water is independent of its rotational mobility.[19] Recent solid-state NMR studies also provided strong evidence for the coupling between the motion of the water and protein backbone.[20]

In order to probe the rapidly diffusing surface water near DNA, we must overcome two obstacles. First, we must selectively detect the dynamics of water at the surface of DNA. Second, we must separate contributions of freely diffusing water from those of the more slowly moving water molecules that bound to or chemically exchanging with the DNA (*i.e.*, “bound/exchanging water”).

We implement highly localized measurements by leveraging techniques that have been developed for electron spin resonance (ESR) studies[21] to attach nitroxide spin labels to

specific sites on DNA, then probe the nearby water molecules with an emerging NMR-ESR double-resonance relaxometry method called Overhauser effect Dynamic Nuclear Polarization (ODNP). ODNP measures the enhancement (i.e. hyperpolarization) of the NMR signal of mobile water molecules in response to the excitation of the ESR transition of the nitroxide spin probe, here 9.8 GHz at a 0.35 T magnetic field. These signal enhancements, in combination with the NMR T_1 relaxation rates, allow one to observe the diffusive dynamics of hydration water within 5 – 15 Å of the spin label (as described in more detail in the Methods and SI Section S3.1).[10,22] Herein, we acquire data for nine different spin labeled DNA samples.

With a new ODNP analysis protocol, we are able to separate dynamics on the tens to hundreds of picosend timescale from dynamics occurring at the nanosecond to tens of nanosecond timescale. The former, fast dynamics arise almost exclusively from water that translates past the spin label. The latter, slow dynamics arise from bound/exchanging waters. We thus observe the faster water dynamics against a significant background of slower proton motions.

Recent studies of protein and lipid vesicle surfaces have routinely shown retarded hydration dynamics that are distinct from the dynamics of the bulk, whether these studies have been performed by ODNP,[23,24] IR,[25,26] dynamic Stokes Shift,[1] neutron relaxation[27,28] or THz spectroscopy,[29,30] – an incomplete list by far. In contrast to protein or liposome surfaces, our study finds that the DNA surface is predominantly hydrated by water that freely diffuses with correlation times nearly indistinguishable from the correlation time of bulk water. The bulk-like property of this surface water implies a low energetic barrier for displacement and dehydration that may play a functional role in mediating the interaction between DNA and its partners.

Materials and Methods

DNA synthesis and spin-labeling

All DNAs (Fig. 1(a)) were synthesized by solid-phase chemical synthesis and obtained commercially (Integrated DNA Technologies, Coralville, IA).

To attach the R5 (Fig. 1(b)) label,[31] a phosphorothioate-modified DNA strand (∼ 300 μM) was reacted with a nitroxide precursor, 3-iodomethyl-2,2,5,5-tetramethyl-1-oxylpyrroline (200 mM), in an aqueous solution (50 μL) containing 0.1 M MES (pH=5.8) and 40% acetonitrile. After incubating in the dark at room temperature and under constant shaking for 12h, the labeled DNAs were purified by anion-exchange HPLC followed by desalting using a reverse-phase column.[21] The desalted oligonucleotides were then lyophilized, resuspended in water and stored at -20°C. Note that all data reported were acquired without separating the Rp and Sp phosphorothioate diastereomers present at each attachment site.

To attach R5a, the same procedure was employed, except with the nitroxide precursor 4-bromo-3-bromomethyl-2,2,5,5-tetramethyl-1-oxylpyrroline and an incubation time of 24h.

The stock concentration of DNA was determined by absorbance at 260 nm, using extinction coefficients of 108,200 $M^{-1}cm^{-1}$, 125,800 $M^{-1}cm^{-1}$, 232,300 $M^{-1}cm^{-1}$, and 230,500 $M^{-1}cm^{-1}$ for the 12bp sequence A-chain, 12bp sequence B-chain, 24bp sequence A-chain, and 24bp sequence B-chain, respectively (see Fig. 1(a)). Note that these extinction coefficients are not dependent on R5/R5a or biotin attachment.

DNP sample preparation

DNA duplexes for DNP measurements were prepared by mixing a labeled strand with the appropriate complementary strand at a molar ratio of 1 to 1.1. To anneal the duplex, the mixture was heated at 95°C for 1 min and cooled at room temperature for 1 min. Salts were then added to reach a final concentration of 50 mM Tris-HCl (pH=7.5) and 100 mM NaCl, with the labeled DNA duplex at 200 μM. This mixture was kept at room temperature for at least 1h to allow for duplex formation, which was verified by native gel shift assay and by ESR lineshape analysis (data not shown).

The DNA duplexes were tethered to streptavidin following a procedure that allows complete DNA attachment.[32] Specifically, a labeled DNA duplex (annealed as described above with a biotin-containing unlabeled strand – Fig. 1(a), sequences 2-4) was mixed with streptavidin (Amresco, Solon, OH) at a molar ratio of 1 to 1.5 (DNA duplex *vs*. streptavidin monomer). The final sample contained 200 μM streptavidin-tethered, labeled DNA duplex, 50 mM Tris·HCl (pH=7.5), and 100 mM NaCl. Before conducting ESR and DNP measurements, the sample was incubated at room temperature for 2h.

Complete tethering of biotinylated DNA duplex onto streptavidin was confirmed by native gel shift assay and ESR lineshape analysis (Fig. S2). Under our experimental conditions, streptavidin tetramerizes,[33] resulting in four labeled DNA duplexes tethered to a streptavidin complex. Control studies showed that the spectroscopic measurements reported in this work were not impacted by possible inter-spin interactions within the same tetramer. In addition, in all DNP samples, the amount of spin label detached from the DNA duplex was estimated to be less than 5% of the total spin population (Fig. S3), and therefore has a negligible effect on the ODNP results.

We note that the DNA sequences chosen in Fig. 1(a) have been well characterized by previous studies, shown to be B-form DNA, and are chosen such that spin-labeled strands will not form duplexes with each other, thus allowing for one spin label per duplex. Furthermore, circular dichroism, molecular dynamics, and a comparison between ESR distance measurements and NMR-derived structure all verify that the spin labeling of these sites does not affect the DNA structure.[34,35]

X-band ESR spectroscopy

For each X-band continuous-wave (cw-) ESR spectrum, ∼ 5 μL sample was loaded into a 0.6 mm i.d. × 0.8 mm o.d. glass capillary (Vitrocom, Inc., Mountain Lakes, NJ), sealed at one end. The spectra were acquired on a Bruker EMX spectrometer using a dielectric ER4119HS cavity, an incident microwave power of 2 mW, and a field modulation of 1 G at

100 kHz. The measured averaged ESR spectra were base-line corrected and normalized following previously described procedures.[36]

The effective rotational correlation time, τ_R, of the nitroxide tethered to the DNP samples (in units of s) was estimated from the ESR line-shape as previously described:[37]

$$\tau_R(s) = 6.5 \times 10^{-10} \Delta H_0 \left(\sqrt{\frac{h(0)}{h(-1)}} - 1 \right) \quad (1)$$

where ΔH_0 is the peak-to-peak linewidth of the central line in Gauss, and $h(0)$ and $h(-1)$ are the peak-to-peak amplitudes of the central and high field lines, respectively.

ODNP: experimental

A home-built NMR probe was inserted into a 3 mm o.d. ESR tube located inside a TE011 (cylindrical) ESR cavity (ER 4119HS-LC from Bruker, Billerica, MA). The probe fits inside the 3 mm tube and consists of teflon supports holding a 0.8 mm o.d. capillary tube and a simple pair of copper wire hairpin loops. To avoid sample heating, the size of the sample was reduced to 3.0-3.5 μL. The entire setup was positioned inside the gap of a commercial ESR magnet (Bruker EMXplus) and air was flowed through the 3 mm ESR tube at ~9 L/min to stabilize the sample temperature (~ 24°C).

The probe was connected to a tuning circuit and a Bruker Avance NMR console. The NMR signal from the water protons was measured with a standard 90° rf pulse followed by a repetition delay of at least $5 \times T_{1,max}$, where $T_{1,max}$ is the maximum longitudinal relaxation time of the protons in water.[10]

The microwave frequency was matched to the resonance of the critically coupled ESR cavity. The static magnetic field was set by observation of the NMR water resonance, which was verified to coincide with 1.5167%o (*i.e.* parts per thousand) of the central ESR transition of the spin label. The NMR signal level was measured for a series of microwave powers, p, ranging from 0 to 4.5 W. (Microwave power was supplied by a home-built microwave amplifier with a design similar to those previously published.[38]) The ODNP signal enhancements, $E(p)$, were calculated by integrating the baseline- and phase-corrected resonance peaks and normalizing them against the thermal ($E(p = 0) = 1$) signal. For measurements that employed a heating correction, [10] standard inversion-recovery NMR pulse sequences acquired the NMR longitudinal relaxation rate, $T_1(p)$, at 5-8 different levels of microwave power, p, between 0 and 4.5 W. Inversion recovery measurements were also acquired in the absence of microwave power for samples that were prepared both with and without attached spin label, yielding $T_1(p = 0)$ and $T_{1,0}(p = 0)$, respectively.

ODNP analysis

ODNP differs significantly from what we may term “traditional” NMR measurements of hydration dynamics, *e.g.*, NOE (nuclear Overhauser effect) and ROE (rotational frame nuclear Overhauser effect) measurements in aqueous solution[39] in two very important aspects. First, ODNP focuses on measuring the relaxation rates in the vicinity of a (stable)

nitroxide spin label. Because the spin label has an overwhelmingly large gyromagnetic ratio (> 659× greater than ^{1}H), it becomes much easier to isolate and identify the interaction of interest – in this case, the fluctuating interaction between the spin label and the hydration water. Second, ODNP involves the active excitation of the ESR transition, and – in doing so – leads to a signal enhancement whose magnitude depends crucially on timescales that are at least an order of magnitude faster than those relevant to NOE and ROE. While the characteristic frequency associated with the ODNP cross-relaxation is ∼ 9.8 GHz in a 0.35 T magnet, the highest characteristic frequency relevant to an NOE or ROE experiment in a 12 T magnet is only ∼ 1 GHz (*i.e.*, twice the ^{1}H resonance frequency, corresponding to a flip-flip relaxation).

By combining the enhancement and relaxation measurements, one can extract a unitless parameter known as the ODNP coupling factor, ξ (Eqs. (S14)–(S19)). The standard approach to interpreting ξ relies on comparing this ξ value to the predictions of the force-free hard-sphere (FFHS) model[40–43] for a range of different correlation times for translational diffusion (*i.e.* τ_{FFHS} – as illustrated in Fig. 2; for consistency with older measurements, the "uncorrected" values from Table 1 are presented here). In this standard analysis, one uniquely identifies the measured ξ value with a single τ_{FFHS}. The value of τ_{FFHS} (units of ps) can be interpreted as the lifetime of the spin-spin dipolar interaction between the protons of the water molecule and the electron spin of the spin label and scales inversely proportionally with the local diffusivity, D_{local}, of the water near (5-15 Å) the spin label. Upon normalizing the value of τ_{FFHS} for local surface water by the τ_{FFHS} of bulk water, the retardation factor ($\tau_{FFHS}/\tau_{FFHS,bulk} = D_{bulk}/D_{local}$), is obtained (as indicated at the top of Table 1). The FFHS-based standard analysis approach has been successfully used in a wide variety of ODNP experiments to date,[9,10,22,44,45] as well as this work.

In addition, ODNP data presented here are analyzed using a newly developed approach involving two relaxivity values, called k_σ and k_{low} (see Section S2.1 and Section S3.1 and Eqs. (S2), (S4), (S7) and (S8) for details on how these values are obtained and separately evaluated). The values of k_σ and k_{low} are directly calculated from different components of the raw data (*i.e.*, the relaxation times and enhancements), as an intermediate step before calculating ξ. The ratio of k_σ and k_{low} is algebraically and monotonically related to ξ:

$$\xi\left(\frac{k_\sigma}{k_{low}}\right)=\frac{5\frac{k_\sigma}{k_{low}}}{3+7\frac{k_\sigma}{k_{low}}}. \quad (2)$$

where $0 \leq \frac{k_\sigma}{k_{low}} \leq 1$. Linear combinations of relaxivities are chosen to calculate k_σ and k_{low} such that each pertains to motion on a different timescale.

In Eq. (2), the value of k_σ is balanced against the competing self-relaxation rate, $k_\rho C_{SL}=\frac{3}{5}k_{low}C_{SL}+\frac{7}{5}k_\sigma C_{SL}$. This is the rate at which the spin label induces the NMR signal from the water to relax back towards equilibrium (*i.e.* towards an unenhanced signal). It is important to note that methods, such as NMR relaxation dispersion (NMRD), have also

previously been developed to analyze the NMR relaxation rate of spin-labeled macromolecules; these methods typically measure $k_\rho C_{SL}$.[11,46–48] The value of $k_\rho C_{SL}$ depends on the relative motion of the water and spin label at both the ESR frequency of 9.8 GHz (*via* k_σ) and the NMR frequency of 15 MHz (*via* k_{low}). Because k_ρ depends on two diverging timescales, the data analysis for these methods may be subject to ambiguity. ODNP enhancement values provide an additional observable, which, together with NMR T_1 relaxation times, accurately and sensitively determines the k_σ value (Eq. (S15)[10]) which, in turn, offers the unique opportunity to isolate the value of k_{low} (Eqs. (S8) and (S9)) – *i.e.*, the portion of k_ρ that depends only on fluctuations occurring at the slower NMR frequency.

Results

High coupling factor at DNA surfaces

We first carry out ODNP measurements with an R5a nitroxide label (Fig. 1(b)) attached to a backbone position at the center of a 12-bp DNA duplex (Fig. 1(a), first sequence).[21,34] Prior studies have demonstrated that the R5a and R5 probes minimally impact the native conformation of DNA duplexes.[31,34] Molecular modeling[21] indicates that the electron spin on this label resides $\sim$ 10 Å from both the major and minor grooves of the DNA. The DNA surface displays a measured value of the ODNP coupling factor, ξ, of 0.17 (Table 1 (second row)), which exceeds the measured values obtained on a range of biomolecular surfaces using similar nitroxide probes, including protein, polymer and lipid membrane surfaces – all of which fall below 0.15.[10]

We again emphasize two key advantages of ODNP. First, while the underlying principle of extracting water dynamics is the same, magnetic resonance techniques that employ relaxation pathways involving electron spin labels in a given magnetic field[10,11,22,46] necessarily probe a much faster timescale of proton motions than traditional NMR relaxometry experiments.[39,49] Second, the pairwise interaction between the spin label and the protons of the water is uniquely strong, given the high gyromagnetic ratio of the electron spin. This avoids a situation possible in NOE measurements, where many proton-proton interactions might play an important role and lead to the probing of interactions that are – in effect – much longer range.[50]

As mentioned in the Methods section and shown in previous publications[10], in comparison to previous relaxometry techniques, ODNP is more sensitive to and selective for fast (on the scale of tens of ps) motions. In the simplest limit, we can assume that the most significant fast motions are comprised of the translational motion of water nuclei. In this case, the FFHS model[40] for translational diffusion provides the best available means for analyzing such data. The approximation of pure translational diffusion has been shown to be particularly relevant for systems such as lipid vesicles, where Bryant *et. al.*[11] have experimentally shown that the hydration dynamics near lipid vesicles adhere well to a FFHS model. We also expect the pure translational FFHS approximation to be valid when the ns-scale motions of bound/exchanging waters are masked by the fast rotational diffusion of small biomolecules that tumble with correlation times that are faster than the bound water lifetime, as is the case with the 187 residue long tau protein – and other small peptides – or

the 17 kDa ApoMb[23] (which is a fraction of the molecular weight of the streptavidin complex employed in the second part of this study).

Assuming the validity of the standard FFHS-based ODNP analysis approach,[22] one can translate the high coupling factor observed on the surface of DNA directly into a translational correlation time (τ_{FFHS}) of 107 ps that is significantly shorter than nearly all of the values that have been observed previously on other molecular surfaces, as shown by Fig. 2, where the data from DNA are compared against a broad survey of previous ODNP measurements of a variety of sample systems. Fig. 2 also illustrates how all previous measurements can be categorized[10] into one of four zones of "bulk-like," "surface," "intermediate," and "buried," as observed on surfaces or interiors of proteins or other soft materials systems. Because the coupling factor measured here for DNA is so high, it lies in the regime that has been previously labeled as exhibiting fast, "bulk-like" water dynamics.

While the FFHS model thus allows one to draw meaningful comparative conclusions, one must also acknowledge that an incautious application of the FFHS model, even for relative comparisons, can be problematic. Indeed, historically, magnetic resonance studies on hydration dynamics with magnetic resonance-based methods have been challenged by concerns over how the slower, ns-scale motions of bound/exchanging waters might skew the measurement of the rapidly diffusing waters. We can show that this phenomenon has an insignificant effect on the traditional, FFHS-based ODNP analysis over a limited regime of dynamic conditions, and yet can prove quite significant over another regime. In particular, recall that Eq. (2) demonstrates how the value of the coupling factor, ξ, depends monotonically on the ratio of two quantities – *i.e.*, k_σ/k_{low}. The traditional analysis of ODNP data, employed in Fig. 2, assumes that k_σ and k_{low} are only influenced by translationally mobile water that can be modeled by the FFHS model. However, slower ns-scale motions, such as the exchange of loosely bound water molecules and/or the fast chemical exchange of their protons, can potentially affect the value of k_{low}. As noted in Fig. S5 (in the SI), when such slower motions contribute up to 10% of the value of k_{low}, the FFHS model can be employed with reasonable accuracy. However, caution must be exercised to ensure that the slower processes do not contribute significantly to k_{low}.

In our analysis of the ODNP data, we thus must first verify whether the FFHS model provides a valid interpretation of our data. The root concern lies not in the validity of FFHS as a model of freely diffusing water, as *e.g.*, Lorentzian models of fast exchange[51] or models of uniform diffusion[52] would face qualitatively similar issues when multiple timescales are present and must be decoupled in order to obtain an accurate analysis. Rather, we are concerned with the extent to which bound/exchanging waters moving with correlation times of nanoseconds or longer might impact the ODNP measurement aimed to capture the diffusion dynamics of water moving with correlation times in the tens to hundreds of picosecond range.

As a key objective, this paper seeks to firmly prove that the fast diffusion dynamics of water observed near DNA surfaces are an intrinsic property exerted by the DNA surface. We design and perform a series of control experiments in order to exclude experimental or methodological artifacts. Specifically, we deliberately alter the rotational motion of the

DNA, and the contribution of bound/exchanging waters by tethering the DNA to the surface of a large protein and, finally, we alter the flexibility of the attached spin label, to examine whether or not such alterations change the observation of the uniquely fast hydration dynamics.

Rotational immobilization and new analysis techniques

A key challenge in ODNP analysis in general,[53,54] and for this measurement in particular, is to delineate the contribution of the bound/exchanging waters from that of freely diffusing water. The anomalously high ξ values observed on DNA surfaces could arise not only from hydration water whose translational diffusion is minimally retarded, but also from the different sensitivities of the ODNP measurement to bound/exchanging water on DNA *vs*. on protein surfaces. The relatively small ($\sim$ 7.3 kDa) and compact 12-bp DNA duplex likely undergoes fast rotational diffusion on the order of only a few ns.[8,55] Water bound to or exchanging with the DNA on a timescale of $\sim$ 1 ns or longer will therefore diffuse along with the DNA and may contribute to the ODNP coupling factor (ξ) differently than it does for larger, more immobile macromolecules. To address this issue, we develop an experimental strategy that allows us to extricate the bound water contribution, in which a covalently attached biotin tethers the R5a-labeled 12-bp DNA duplex to the surface of a streptavidin tetramer, yielding a macromolecular complex with a molecular weight of approximately 82 kDa. As a result, the global rotational correlation of the complex slows drastically, increasing from a few ns[8,55] to > 20 ns,[56,57] and concomitantly reduces the dynamics of the bound/exchanging waters associated with the DNA. We strategically attach R5a labels, one at a time, to three different locations on the DNA (Figs. 1(a) and 3(a)): the proximal label samples the hydration dynamics at the DNA/streptavidin interface, while the distal and central labels (> 20 Å from the protein surface) report primarily on the hydration dynamics near the DNA surface. Thus, experiments on the tethered complex offer a perfectly controlled comparison between dynamics at the protein surface and dynamics that are representative of the un-pertubed DNA surface (see Fig. 3(a)). We carry out ODNP measurements on both untethered and tethered DNA samples.

For this dataset, we have also acquired additional NMR relaxation data that allow us to correct for moderate residual microwave sample heating and report a heating-corrected value for ξ and $\tau_{FFHS}/\tau_{FFHS,bulk}$[10] (see also Section S3.4). For the untethered DNAs, all three labels give high ξ values (0.17, 0.22, and 0.16, Table 1) that are similar to those of the un-biotinylated DNA (with $\xi \approx$ 0.18, 0.17, and 0.16) and that the standard analysis approach interprets as short τ_{FFHS} values, corresponding to local diffusivities that are close to the diffusivity seen in bulk water[10] (see Table 1, rows 3-6).

Upon tethering, all the measured ξ values reduce to about 52% or less of their original value, and the ξ for the proximal site even decreases to less than 17% of its original value (Table 1: compare rows 3-6 to 7-9). The FFHS model would interpret this decrease as a lengthening of τ_{FFHS}. The standard analysis approach would therefore conclude that the diffusion dynamics of the DNA hydration water (D_{local}/D_{bulk}) slows upon tethering of the DNA to streptavidin. This conclusion is unphysical, since it is unlikely that the presence of the protein alters the DNA surfaces at the distal and central sites. Instead, this apparent slowing

of the hydration water likely arises because the FFHS model employed by the standard approach does not offer separate parameters to account for the contributions from bound/exchanging *vs*. translationally mobile, diffusive, waters. In other words, the presence of bound waters may skew (lengthen) the apparent value of τ_{FFHS} (in the fashion indicated by Fig. S5). To test this hypothesis, we need a method to separately evaluate the dynamics of the slow bound/exchanging *vs*. fast translationally mobile hydration waters.

We develop a new analysis approach that separately determines two relaxivity values, called k_σ and k_{low}, from the ODNP NMR relaxation times and enhancements (Eqs. (S15)–(S17)). The coupling factor (ξ) is a function of these relaxivity values, as given by Eq. (2), and the determination of any of these three quantities (k_σ, k_{low}, or ξ) is model-free. Even a cursory inspection of the data presented in Figs. 3(b) and 3(c) shows that a separate analysis of the two relaxivity parameters allows us to discriminate a qualitatively different behavior at the proximal, protein contacting, site *vs*. the other two sites that resemble the unperturbed DNA surface. Specifically, k_σ decreases to about 3/4 of its original value at the proximal site upon tethering of DNA to streptavidin, while remaining unaltered to within error (less than 10%) at the central and distal sites. In contrast, k_{low} increases to 2.3 and 2.6× its original value at the distal and central sites (respectively) upon tethering of the DNA, and even more dramatically – to 5.9× its original value – at the protein proximal site of the tethered DNA (see also Table 1).

These diverging results are obtained because k_σ and k_{low} probe the dynamic interaction between the water and the spin label at orders of magnitude different timescales, defined by the NMR and ESR frequencies, which in a 0.35 T field are 15 MHz and 9.8 GHz, respectively (*cf*. Eqs. (S2) and (S9)). Similar to other NMR relaxometry approaches, these relaxivity measurements access information on dynamics because the relaxivities are proportional to the spectral density of a spin-based interaction.[58] The spectral density is the statistical mechanical function quantifying the likelihood that an interaction will fluctuate in resonance with a particular frequency. ODNP probes the electron-proton dipolar interaction, and so k_σ and k_{low} both probe the dynamics of proton-bearing water molecules located within 5-10 Å of the electron spin label. The value of $k_\sigma C_{SL}$ (where C_{SL} is the spin label concentration) determines the rate at which the ODNP signal enhancement builds up and only depends on the value of the dipolar spectral density near the ESR resonance frequency. [10,51,59] The period of the ESR frequency (9.8 GHz at 0.35 T) happens to be within the range of times that it typically takes for a translationally mobile, diffusing water molecule to move through the dipolar field generated by the spin label (*i.e.* τ_{FFHS}; note the steep slope of the curve in Fig. 2 for $\tau_{FFHS} \sim 10 - 300$ ps).

To learn how to interpret k_{low} and contrast it with k_σ in order to distinguish between translationally mobile and bound water, we turn to Fig. 4. It illustrates a highly simplified model for the spectral density function that includes interactions between translationally mobile water and the spin label, as well as bound/exchanging water and the spin label. This “toy” model makes the approximation that the rotational motion of the macromolecule provides the primary means for modulating the interactions between the population of bound/exchanging water and the spin label (Section S2.2). The main panel on the right side of Fig. 4 shows the net spectral density function for dipolar interactions between the spin

label and the water of this model system. The contributions to this total spectral density from the translational dynamics of the water *vs*. the rotational dynamics of the water/macromolecule complex are separately depicted in coarse-dashed red *vs*. fine-dashed blue, respectively, and annotated as J_{FFHS} and J_{rot}. The insets to the left demonstrate how simulations of the various measured values (k_σ, k_{low}, and ξ) respond to changes in the rotation of the macromolecule and associated bound water (top) and to changes in the diffusivity of the freely translating water (bottom). These results are calculated from a spectral density function following Eqs. (S1), (S3), (S5) and (S8). Because they sample the spectral density function at 9.8 GHz, measurements of k_σ (solid red lines) apply a short-timescale threshold to the molecular dynamics that they probe and only respond to changes in fast processes – notably, translationally diffusive motion of the water protons (Fig. 4, bottom inset). By contrast, measurements of k_{low} (solid blue lines) sample the spectral density function at 15 MHz and thus apply a much longer timescale threshold. As shown in Fig. 4 (top inset), only the values of k_{low} change in response to altering rotational dynamics, and they increase as rotational motion slows, until they peak when the rotational correlation time matches the proton's Larmor precession, *i.e.* $\tau_{rot} = 1/2\pi 15\ \text{MHz} \approx 11$ ns.

Importantly, changes to the rotational correlation time change not only k_{low}, but necessarily also the coupling factor (ξ – green lines), which depends on k_{low} (*via* Eq. (2)). However, k_σ remains unaltered (Fig. 4, top inset, solid red line). Thus, especially in the presence of dramatic changes to the tumbling dynamics of the macromolecule – such as when we tether a DNA duplex to the streptavidin – we learn that k_σ will more robustly evaluate the modulation and contribution of translationally mobile hydration water. The value of k_σ is independent of the changing contributions from slow waters, such as bound/exchanging waters whose correlation time is modulated primarily by slow molecular tumbling or exchange on and off of the biomolecule on a similar timescale. Tethering can artificially and dramatically slow the rotational correlation time of the DNA, and thus the effective correlation time of the water bound to the DNA (similar to τ_{rot} in Fig. 4) from a few ns or less to up to tens of ns. Thus, macromolecular immobilization, such as the tethering to streptavidin we employ here, is a tool for revealing the presence of bound/exchanging water which will lead to a value of k_{low} that increases without associated changes to the value of k_σ.

One can interrogate the translationally mobile *vs*. bound hydration water surrounding DNA by separately analyzing the values of k_σ *vs.* k_{low} in Figs. 3(b) and 3(c). This experiment comprises four datapoints for each of the three spin label sites (namely, k_σ and k_{low}, both free and tethered). At the site proximal to the protein surface, we observe that k_σ decreases by 28% upon tethering, a change which we propose arises primarily from the spin label packing against the surface of the protein (see Fig. 3(a), bottom right) and thus sampling, to some extent, the protein's surface hydration properties. This spin label-protein interface packing is also evidenced by the appearance of an extra immobile component in the ESR spectrum of the proximal label (Fig. S2(c)). In contrast, the values of k_σ probed by the two DNA surface labels (distal and central label positions) both change by less than 11% (Fig. 3(b) and Table 1), informing us that the dynamics of the fast water near DNA remain consistently rapid. As expected, the extraordinarily fast dynamics of the translationally

mobile hydration water do not depend significantly on the macromolecular tumbling, and thus are a genuine feature intrinsic to the DNA surface. As evidenced by the observation that k_σ remains unchanged, (*cf*. Eq. (2)) the apparent change in ξ that we observe upon tethering is not instigated by changes in the diffusivity of the freely translating hydration water. Rather, the slower macromolecular rotation that emphasizes the contribution from the bound/exchanging water (*i.e*., increases the value of k_{low}) induces this change in $\xi(k_\sigma/k_{low})$. Therefore, the τ_{FFHS} values that the standard analysis approach estimates for the untethered DNA samples (Table 1 rows 1-6), whose bound water contribution is masked by fast tumbling, are indeed valid in representing the characteristics of the fast translational diffusivity of surface hydration water, while the τ_{FFHS} values of the tethered DNA sample would be artificially lengthened by the presence of bound/exchanging waters. (The associated retardation times predicted by FFHS would be 3.65, 2.94, and 7.63 for the distal, central, and proximal label sites, respectively; for clarity, they are not included in the Table 1 and Fig. 3(c) since FFHS model is not expected to reasonably model the translational correlation times of the tethered complexes.)

In additional tests, the significant presence of “bulk-like” water around untethered DNA, with ξ values between 0.16-0.18, was verified to remain unchanged upon doubling the length of the un-tethered DNA duplex (12 b.p. duplex $\rightarrow$ 24 b.p. duplex) as well as increasing spin label flexibility. (More details of this test are described by Fig. 1(b) and SI Section S3.5.) This observation indicates that the “bulk-like” water is not an artifact due to peculiar features of the spin labeled DNAs used in the ODNP measurements.

Discussion

An ODNP analysis that separates dynamics occurring at different timescales

Here, we present a novel approach, in which the information from k_σ, k_{low}, and careful experimental design combine synergistically to deliver a clear interpretation of the results on the DNA hydration water dynamics. For instance, the value of k_σ can depend on the local accessibility of the spin label to water, so it is important to ensure that the local accessibility changes minimally – as we have done here by carefully selecting labeling sites and redundantly labeling the tethered DNA. Furthermore, a retardation of either translational or bound/exchanging water dynamics (*cf*. Fig. 4) can increase the value of k_{low}, so an observation of a concerted increase or concerted decrease in k_σ and k_{low} can imply an ambiguous result. However, if – as here – one can design a change to the chemical system such that only k_{low} changes (Fig. 3(c)), while k_σ remains constant (Fig. 3(b)), one can attribute the increasing k_{low} to changes of the slow-timescale, *i.e*. bound/exchanging water, dynamics. The resulting $\sim$ 130 – 160% increase in k_{low} at the central and distal sites (Table 1 and Fig. 3(c)) clearly points to the presence of bound/exchanging water located near the spin label on the surface of DNA. Finally, Fig. 3(c) (and Table 1) show an increase of k_{low} by $\sim$ 490% for the protein-contacting (proximal) spin label that accompanies the previously mentioned decrease in k_σ. This suggests that the protein surface induces further retardation of translational dynamics and/or presents a higher quantity of bound water than on the DNA surface under identically controlled conditions.

The value of k_{low}, which arises in part from bound water, is > 2.6 – 2.7× smaller at the tethered DNA surface sites (distal and central) than at the protein exposed (proximal) site (Fig. 3(c), blue bars). Thus, even the contribution from bound water at the DNA site can be identified as less dominant than on the streptavidin surface to begin with. In untethered DNA, this value of k_{low} drops by another factor of ∼ 2.3 – 2.6× (*cf*. Fig. 3(c), red *vs*. blue bars for distal and central samples). This reveals that, even though bound/exchanging water already contributes less dominantly than on protein surfaces to begin with, the free rotation of the unmodified (*i.e*., untethered) 12-b.p. DNA additionally "hides" contributions from bound water, and thus predominantly displays the dynamics of freely diffusing hydration water.

For this and other sample systems, we thus advocate an analysis procedure that relies on two steps. First, we develop model-independent insights into the presence of bound water by analyzing changes in k_σ and k_{low}, and we thus determine the applicability of the FFHS model for translational dynamics. Then, when justified, we can proceed by employing the FFHS model to convert the value of $\xi(k_\sigma/k_{low})$ (Eq. (2)) into a correlation time, τ_{FFHS}, for the translational diffusion of water near the spin label.[22] The standard FFHS-based analysis allows us to calculate the retardation in solvent dynamics ($\tau_{FFHS}/\tau_{FFHS,bulk}$) and compare to similar, previous ODNP measurements, where the retardation factor on macromolecular surfaces were typically found to be > 3-fold.[23,24,53,60,61] As already noted, these previously analyzed surfaces include both those that have been shown to have hydration dynamics that adhere well to the FFHS model for translational dynamics, as well as those that are expected to adhere well to FFHS dynamics due to sufficiently fast molecular tumbling.

This shows that the water near the surface of the DNA moves with a correlation time (τ_{FFHS}) only 2.0× longer than that of bulk water (Fig. 2). The recently observed, and exceptionally fast, hydration water on the surface of GroES[62] comes closest to this value with ∼ 2.3-fold retardation ($\tau_{FFHS}/\tau_{FFHS,bulk}$), while more typically observed values are represented by a > 3-fold retardation for the hydration water of monomeric peptides[61] or a greater than 5-fold retardation seen on typical protein surfaces[23] (Fig. 2). As Fig. 2 illustrates, the coupling factor measurement is very sensitive to, and changes dramatically in response to a retardation factor of 2 *vs*. 2.3, 3, or 4.

Looking forward, the analytical models that describe this data could be improved. Previous literature has shown the value of incorporating the discrete nature of water and, accordingly, models have been developed to incorporate the explicit form of water structure in the form of the pair correlation function,[40] to model the interplay between rotational and translational motions,[49] and to account for the off-centered location of proton spins in the water molecule. [63–65]

"Soft" water at the DNA surface

We can conclude that, in dilute aqueous solution, DNA harbors a significant population of hydration water that diffuses unusually rapidly compared to hydration water near the surfaces of proteins or lipid membranes, despite the presence of bound/exchanging waters. We can refer to this DNA surface hydration water as being "softer," since it costs less activation energy to translate and change the position of this water, which necessarily

involves breaking and reforming several hydrogen bonds with several neighboring water molecules.

Multiple observations support this conclusion. First, for the untethered duplexes, the measured ODNP coupling factors (ξ), which are largely invariant with respect to changes in the dynamics of the DNA or the spin label moiety, are high and the FFHS-based standard analysis (see discussion on validity in prior section), translates these to a retardation factor of only $\sim 1.4 – 2.1$, which – likewise – indicates the observation of uniquely fast diffusion dynamics. Importantly, even though the water molecules do move on a timescale of tens of picoseconds, their mobility, *i.e.*, their dynamic structure, can be quite important since it hints at the underlying collective fluctuations that modulate binding and interaction events.[17,18,66]

Second, with the tethering scheme and the new ODNP analysis approach, we observe a signature from some bound/exchanging waters near the DNA surface – signified by the increase in k_{low} upon tethering, as shown in Fig. 3(c). This identification of the existence of a bound/exchanging water population on the DNA surface is consistent with previous literature reports.[8,67] Importantly, even though this signature of bound/exchanging water appears at all three sites – including the DNA surface sites (Fig. 3(c)), it is far less significant (in both magnitude and change) at the central and distal sites than at the protein-exposed, proximal site.

The high mobility of the solvation water around DNA may have been tailored to its role in biological function. One commonly discussed theory of protein binding has proposed that the entropically favorable release of bound water molecules at protein interfaces drives ligand binding and/or conformational changes.[68,69] As such, the variety in the dynamics of the surface hydration water associated with proteins, which ranges from slow to fast, as revealed by ODNP and other measurements,[9,23] is favorable for a high degree of molecular specificity. By contrast, data reported here indicate that DNA would seem to gather about it a larger population of significantly faster, more freely translating water molecules, presenting diffusion dynamics not significantly different from bulk water. The small difference between these “softer” waters and the bulk-like (*i.e.*, the least impeded) water necessarily compresses the range of variation in entropy that can be released as potential binding partners push the soft water near the DNA backbone out of the way. This likely implies a concomitant reduction in the variability and/or specificity of any macromolecular interactions or rearrangements that can be driven by the entropic release of bound water or regulated by heterogeneities in the repulsive forces of surface water. The overall resemblance of hydration dynamics on DNA surfaces to bulk water likely also facilitates the initial approach[18] between the DNA duplex structure and other biomolecules in a relatively nonspecific fashion. This again contrasts with proteins, whose slowest waters can store significant free energy that is entropically released upon binding.[69] A smaller dynamic variety in the surface water dynamics of DNA duplexes would be sensible, since they participate in many processes where they must function relatively similarly. For instance coiling and sliding in the nucleosome[70] and transcription of DNA both rely to a large extent on the DNA presenting a consistent or homogeneous interaction surface.

Conclusion

This work presents a robustly applicable ODNP modality that analyzes hydration dynamics following two general strategies: (1) the model-free analysis provided by the separate analysis of k_σ and k_{low}, and (2) the experimental strategy of employing tethering or other forms of immobilization[71] to tune the contributions from bound/exchanging water. The measurements and analysis reveal a significant presence of *soft* water around DNA surfaces. Such distinct dynamics of the solvation water around proteins *vs*. DNA may be in keeping with the fundamentally divergent roles that the two types of macromolecules play in the central dogma of molecular biology.

Supplementary Material

Refer to Web version on PubMed Central for supplementary material.

Acknowledgments

The authors thank Dr. A. Popova for preparation of the initial spin-labeled DNAs, as well as Dr. J. Song for useful scientific discussions, and J. A. Scott for experimental assistance. This work was supported by the NSF IDBR (DBI-1152244) and the 2011 NIH Innovator award awarded to SH, and the NSF MCB-0546529 and CHE-1213673 awarded to PZQ. JMF acknowledges support by the Elings Prize Postdoctoral Fellowship in Experimental Science from the California Nanosystems Institute (CNSI). This project made use of the UCSB MRL Shared Experimental Facilities, which are supported by the MRSEC Program of the National Science Foundation under award NSF DMR 1121053; a member of the NSF-funded Materials Research Facilities Network (www.mrfn.org).

References

1. Zhong D, Pal SK, Zewail AH. Chem Phys Lett. 2011; 503:1–11.
2. Fogarty AC, Duboué-Dijon E, Sterpone F, Hynes JT, Laage D. Chem Soc Rev. 2013; 42:5672–83. [PubMed: 23612685]
3. Sterpone F, Stirnemann G, Laage D. J Am Chem Soc. 2012; 134:4116–9. [PubMed: 22335572]
4. Pal SSSK, Zhao L, Zewail AHA. Proc Natl Acad Sci. 2003; 100:8113–8. [PubMed: 12815094]
5. Chen S, Liu L, Chu X, Zhang Y, Fratini E, Baglioni P, Faraone A, Mamontov E. J Chem Phys. 2006; 125:171103. [PubMed: 17100421]
6. Khodadadi S, Roh JH, Kisliuk A, Mamontov E, Tyagi M, Woodson SA, Briber RM, Sokolov AP. Biophys J. 2010; 98:1321–6. [PubMed: 20371332]
7. Sokolov A, Roh J, Mamontov E, García Sakai V. Chem Phys. 2008; 345:212–218.
8. Denisov VP, Carlström G, Venu K, Halle B. J Mol Biol. 1997; 268:118–36. [PubMed: 9149146]
9. Ortony JH, Cheng CY, Franck JM, Kausik R, Pavlova A, Hunt J, Han S. New J Phys. 2011; 13:015006.
10. Franck JM, Pavlova A, Scott Ja, Han S. Prog Nucl Magn Reson Spectrosc. 2013; 74:33–56. [PubMed: 24083461]
11. Hodges MW, Cafiso DS, Polnaszek CF, Lester CC, Bryant RG. Biophys J. 1997; 73:2575–9. [PubMed: 9370451]
12. Russo D, Hura G, Head-Gordon T. Biophys J. 2004; 86:1852–1862. [PubMed: 14990511]
13. Jamadagni SN, Godawat R, Garde S. Annu Rev Chem Biomol Eng. 2010; 2:110301095446013.
14. Garde S. Nature. 2015; 517:7–9. [PubMed: 25557696]
15. Patel AJ, Varilly P, Jamadagni SN, Hagan MF, Chandler D, Garde S. J Phys Chem B. 2012; 116:2498–503. [PubMed: 22235927]
16. Heyden M, Tobias DJ. Phys Rev Lett. 2013; 111:218101. [PubMed: 24313531]
17. Willard AP, Chandler D. J Phys Chem B. 2008; 112:6187–92. [PubMed: 18229916]
18. Chong SH, Ham S. Proc Natl Acad Sci. 2012; 109:7636–41. [PubMed: 22538814]

19. Schirò G, Fichou Y, Gallat FX, Wood K, Gabel F, Moulin M, Härtlein M, Heyden M, Colletier JP, Orecchini A, Paciaroni A, Wuttke J, Tobias DJ, Weik M. Nat Commun. 2015; 6:6490. [PubMed: 25774711]
20. Lewandowski JR, Halse ME, Black-ledge M, Emsley L. Science. 2015; 348:578–581. [PubMed: 25931561]
21. Qin PZ, Haworth IS, Cai Q, Kusnetzow AK, Grant GPG, Price EA, Sowa GZ, Popova A, Herreros B, He H. Nat Protoc. 2007; 2:2354–65. [PubMed: 17947978]
22. Armstrong BD, Han S. J Am Chem Soc. 2009; 131:4641–7. [PubMed: 19290661]
23. Armstrong BD, Choi J, López CJ, Wesener DA, Hubbell W, Cavagnero S, Han S. J Am Chem Soc. 2011; 133:5987–5995. [PubMed: 21443207]
24. Franck JM, Scott JA, Han S. J Am Chem Soc. 2013; 135:4175–8. [PubMed: 23347324]
25. King JT, Kubarych KJ. J Am Chem Soc. 2012; 134:18705–12. [PubMed: 23101613]
26. King GM, Carter AR, Churnside AB, Eberle LS, Perkins TT. Nano Lett. 2009; 9:1451–6. [PubMed: 19351191]
27. Benedetto A. Biophys Chem. 2013; 182:16–22. [PubMed: 23953400]
28. Russo D, Murarka RK, Copley JRD, Head-Gordon T. J Phys Chem B. 2005; 109:12966–75. [PubMed: 16852609]
29. Meister K, Ebbinghaus S, Xu Y, Duman JG, DeVries A, Gruebele M, Leitner DM, Havenith M. Proc Natl Acad Sci. 2013; 110:1617–22. [PubMed: 23277543]
30. Bye JW, Meliga S, Ferachou D, Cinque G, Zeitler JA, Falconer RJ. J Phys Chem A. 2014; 118:83–8. [PubMed: 24328100]
31. Popova AM, Kálai T, Hideg K, Qin PZ. Biochemistry. 2009; 48:8540–50. [PubMed: 19650666]
32. Ding Y, Zhang X, Tham KW, Qin PZ. Nucleic Acids Res. 2015; 42:e140. [PubMed: 25092920]
33. Sano T, Cantor CR. Proc Natl Acad Sci. 1995; 92:3180–3184. [PubMed: 7724536]
34. Cai Q, Kusnetzow AK, Hubbell WL, Haworth IS, Gacho GPC, Van Eps N, Hideg K, Chambers EJ, Qin PZ. Nucleic Acids Res. 2006; 34:4722–30. [PubMed: 16966338]
35. Price EA, Sutch BT, Cai Q, Qin PZ, Haworth IS. Biopolymers. 2007; 87:40–50. [PubMed: 17538992]
36. Zhang X, Cekan P, Sigurdsson ST, Qin PZ. Methods Enzymol. 2009; 469:303–28. [PubMed: 20946796]
37. Qin PZ, Butcher SE, Feigon J, Hubbell WL. Biochemistry. 2001; 40:6929–6936. [PubMed: 11389608]
38. Armstrong BD, Lingwood MD, McCarney ER, Brown ER, Blümler P, Han S. J Magn Reson. 2008; 191:273–81. [PubMed: 18226943]
39. Otting G, Liepinsh E, Wüthrich K, Wuthrich K. Science. 1991; 254:974–980. [PubMed: 1948083]
40. Hwang LLP, Freed JHJ. J Chem Phys. 1975; 63:4017–4025.
41. Hwang LP, Freed JH. J Chem Phys. 1975; 63:118.
42. Freed JH. J Chem Phys. 1978; 68:4034–4037.
43. Ayant Y, Belorizky E, Aluzon J, Gallice J. J Phys. 1975; 36:991–1004.
44. McCarney ER, Armstrong BD, Kausik R, Han S. Langmuir. 2008; 24:10062–72. [PubMed: 18700788]
45. Armstrong BD, Han S. J Chem Phys. 2007; 127:104508. [PubMed: 17867762]
46. Polnaszek CF, Bryant RG. J Chem Phys. 1984; 81:4038–4045.
47. Diakova G, Goddard Y, Korb JP, Bryant RG. J Magn Reson. 2011; 208:195–203. [PubMed: 21134772]
48. Diakova G, Goddard YA, Korb JP, Bryant RG. Biophys J. 2010; 98:138–46. [PubMed: 20085726]
49. Brüschweiler R, Wright PE. Chem Phys Lett. 1994; 229:75–81.
50. Halle B. J Chem Phys. 2003; 119:12372.
51. Bennati M, Luchinat C, Parigi G, Türke MT. Phys Chem Chem Phys. 2010; 12:5902–10. [PubMed: 20458388]

52. Abragam, A. The Principles of Nuclear Magnetism. Clarendon Press; Oxford, England: 1961. p. 301-302.
53. Hussain S, Franck JM, Han S. Angew Chem, Int Ed Engl. 2013; 52:1953–8. [PubMed: 23307344]
54. Doll A, Bordignon E, Joseph B, Tschaggelar R, Jeschke G. J Magn Reson. 2012; 222:34–43. [PubMed: 22820007]
55. Kuwata K, Liu H, Schleich T, James TL. J Magn Reson. 1997; 128:70–81. [PubMed: 9345778]
56. Luschtinetz F, Dosche C, Kumke MU. Bioconjugate Chem. 2009; 20:576–82.
57. Maliwal BP, Fudala R, Raut S, Kokate R, Sørensen TJ, Laursen BW, Gryczynski Z, Gryczynski I. PloS one. 2013; 8:e63043. [PubMed: 23667570]
58. Solomon I. Phys Rev. 1955; 99:559–565.
59. Hausser KH, Stehlik D. Adv Magn Reson. 1968; 3:79–139.
60. Cheng CY, Han S. Annu Rev Phys Chem. 2013; 64:507–32. [PubMed: 23331309]
61. Pavlova A, McCarney ER, Peterson DW, Dahlquist FW, Lew J, Han S. Phys Chem Chem Phys. 2009; 11:6833–9. [PubMed: 19639158]
62. Franck JM, Sokolovski M, Kessler N, Matalon E, Gordon-Grossman M, Han SI, Goldfarb D, Horovitz A. J Am Chem Soc. 2014; 136:9396–403. [PubMed: 24888581]
63. Ayant Y, Belorizky E, Fries P, Rosset J. J Phys. 1977; 38:325–337.
64. Fries P, Belorizky E. J Phys. 1978; 39:1263–1282.
65. Albrand JP. J Chem Phys. 1983; 78:5809.
66. Miller TF, Vanden-Eijnden E, Chandler D. Proc Natl Acad Sci. 2007; 104:14559–64. [PubMed: 17726097]
67. Sunnerhagen M, Denisov VP, Venu K, Bonvin AM, Carey J, Halle B, Otting G. J Mol Biol. 1998; 282:847–858. [PubMed: 9743631]
68. Oshima H, Yasuda S, Yoshidome T, Ikeguchi M, Kinoshita M. Phys Chem Chem Phys. 2011; 13:16236–46. [PubMed: 21842056]
69. Nucci NV, Pometun MS, Wand AJ. J Am Chem Soc. 2011; 133:12326–9. [PubMed: 21761828]
70. Schiessel H. Eur Phys J E. 2006; 19:251–62. [PubMed: 16453064]
71. López CJ, Fleissner MR, Guo Z, Kusnetzow AK, Hubbell WL. Protein Sci. 2009; 18:1637–52. [PubMed: 19585559]
72. Cheng CY, Wang JY, Kausik R, Lee KYC, Han S. J Magn Reson. 2012; 215:115–9. [PubMed: 22230738]
73. Kausik R, Han S. J Am Chem Soc. 2009; 131:18254–6. [PubMed: 19791740]
74. Kausik R, Han S. Phys Chem Chem Phys. 2011; 13:7732–46. [PubMed: 21423982]
75. Kausik R, Srivastava A, Korevaar PA, Stucky G, Waite JH, Han S. Macromolecules. 2009; 42:7404–7412. [PubMed: 20814445]

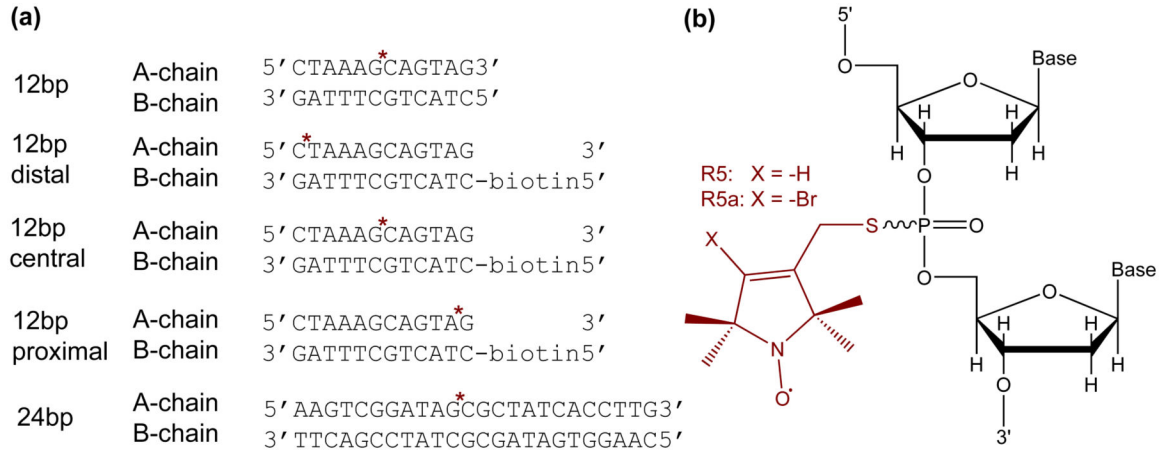

Figure 1.

(a) Sequence of DNA duplexes used for DNP measurement. "*" indicates the location at which a phosphorothioate modification was introduced between the adjacent nucleosides to enable subsequent spin label attachment. **(b)** Chemical structure of the R5 and R5a spin label.

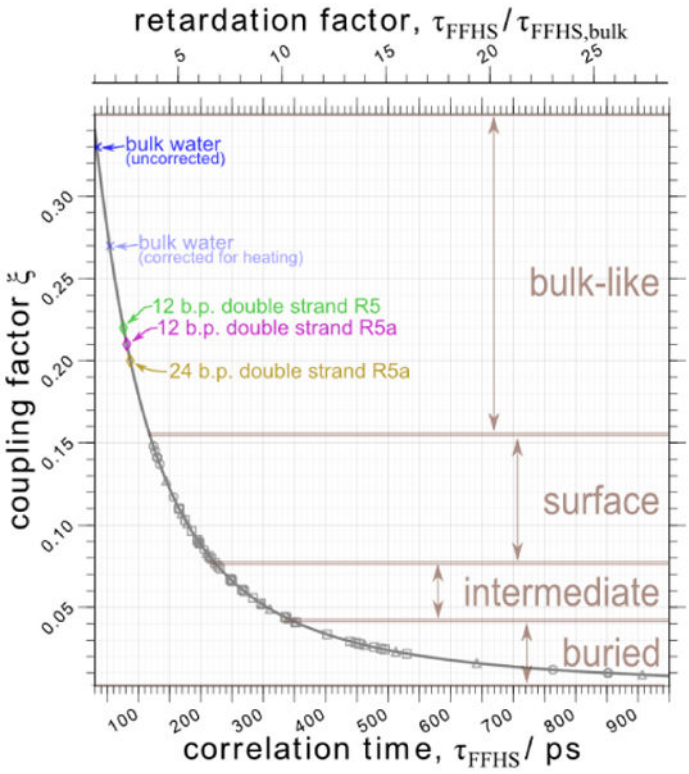

Figure 2.

Experimentally obtained coupling factors, ξ, are presented as symbols. The gray curve presents the relationship between ξ and the translational correlation time (τ_{FFHS} – along the *x*-axis) that is calculated from the force-free hard sphere model[40] *via* an established analysis approach. [10,22,45] The coupling factors for DNA samples (shown in color) are significantly higher than the majority of coupling factors recorded in previous literature (shown in gray[9,23,61,72–75]), and lie in a regime that has been labeled previously as “bulk-like” dynamics.[10] Note that we have excluded measurements taken in this study where there is evidence that the FFHS model approximation is not valid.

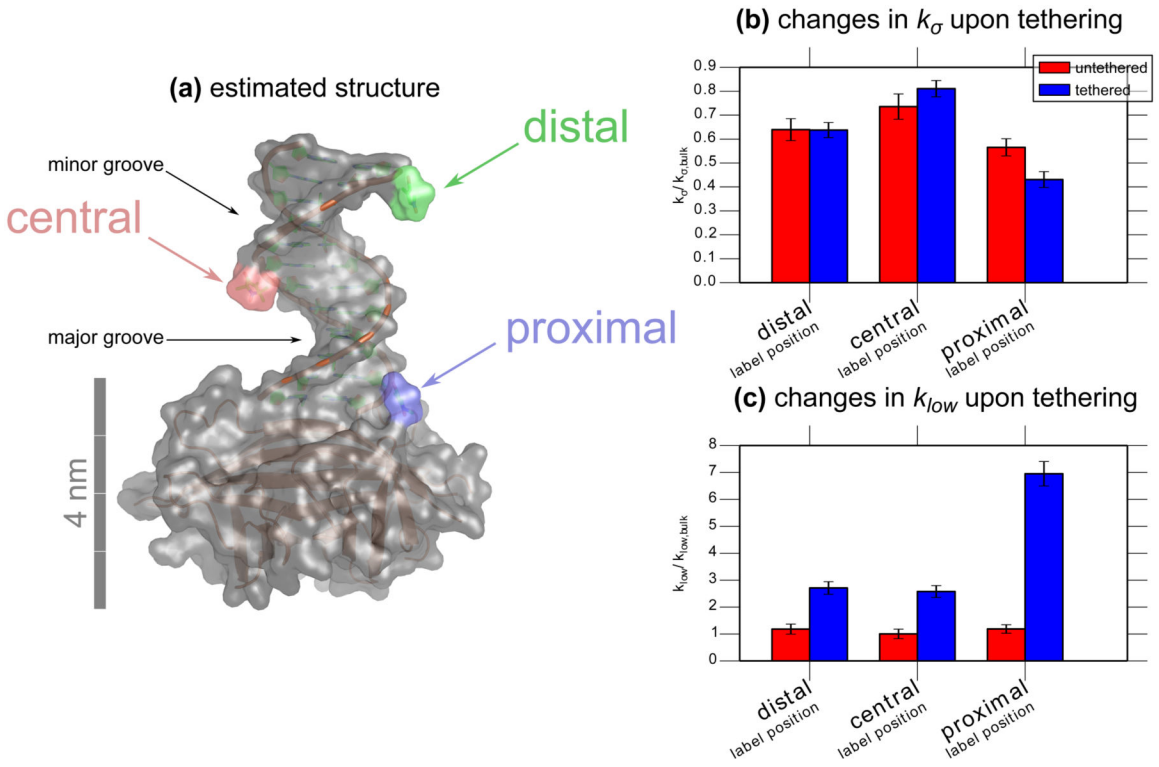

Figure 3.

(a) Shows a representation of the expected solvent excluded surface of the DNA-streptavidin complex. For clarity, only one sub-unit of the tetrameric complex is shown. All three attached spin labels are shown at once, although in each measurement only one label was present in a given sample. **(b)** Shows how the fast-motion relaxivity, k_σ, remains relatively unperturbed after tethering to the streptavidin, decreasing significantly only for the site closest to the streptavidin protein. **(c)** Shows how the slow-motion relaxivity, k_{low}, increases substantially when the DNA is tethered to the streptavidin. This increase is correlated with the presence of bound or exchanging waters, and is much more dramatic for the protein-exposed proximal label position than it is for the DNA surface labels at the distally and centrally located positions. The values of k_σ and k_{low} here are referenced against the corresponding values measured for a small spin label freely dissolved in bulk water:[10] $k_{\sigma,bulk} = 95.4\ s^{-1}M^{-1}$ and $k_{low,bulk} = 366\ s^{-1}M^{-1}$.

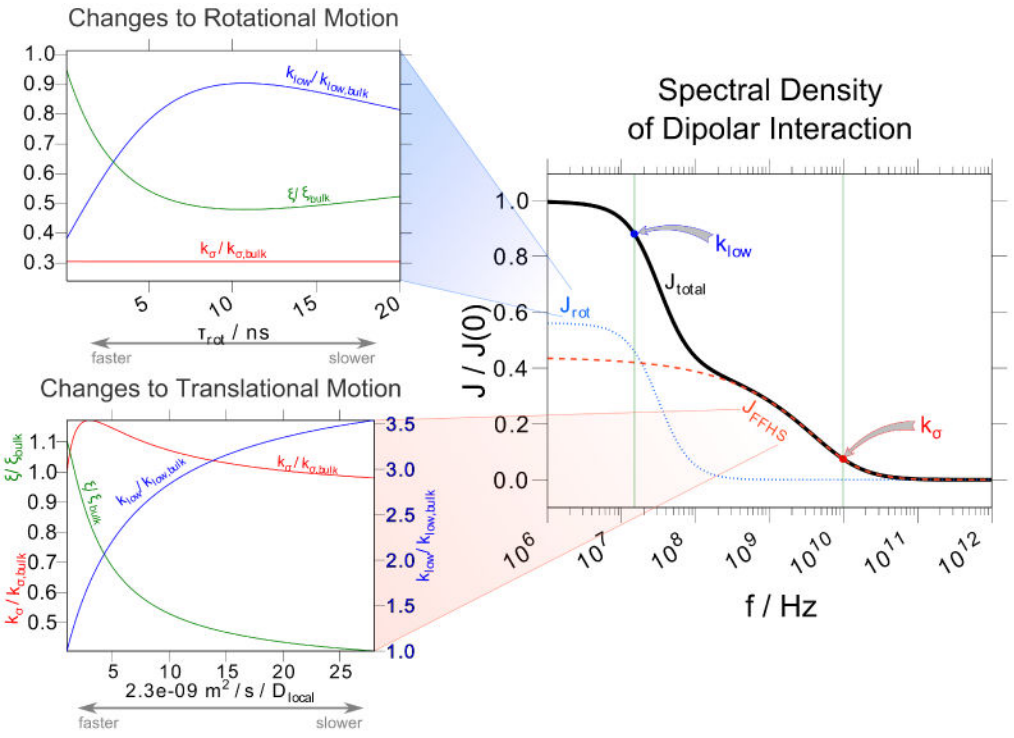

Figure 4.

shows a sample spectral density function designed as a basic "toy" model for a system with both bound and freely translating water. The overall spectral density function, J_{total}, is a linear combination of a rotational component (representing bound water), J_{rot}, and a translational component, J_{FFHS}, as explained in the text. The insets to the left show how the experimental parameters k_{low}, k_{σ}, and ξ vary in response to changes in the bound water dynamics (top inset) and the dynamics of the freely translating water (bottom inset). For convenience, and to make the values unitless, all predicted measurements are normalized by the calculated value for free spin label dissolved in bulk water. As noted, all numbers in the left insets are scaled by the appropriate quantity measured[10] for bulk water. In the top inset, the *y*–axis for all the lines is the same; in the bottom inset, the *y*–axis for k_{low} is slightly different, and shown separately.

Table 1

ODNP measurements on DNA duplexes.

	Sample[a]	ξ/0.01		$\tau_{FFHS}/\tau_{FFHS,bulk}$		$k_\sigma \approx k_\sigma s_{max}$/s^{-1}M^{-1}		k_{low}/s^{-1}M^{-1}	
		uncorrected	corrected	uncorrected[b]	corrected[c]	uncorrected	corrected	uncorrected	corrected
not biotinylated	12-bp duplex R5, central	22.5 ± 3.4[d]	18[e]	2.27 ± 0.53	1.9[e]	96 ± 11	77[e]	510 ± 170	532[e]
	12-bp duplex R5a, central	20.6 ± 3.5	17[e]	2.5 ± 0.5	2.0[e]	83 ± 9	66[e]	480 ± 90	504[e]
	24-bp duplex R5a, central	19.7 ± 3.5	16[e]	2.68 ± 0.5	2.1[e]	86.0 ± 9	69[e]	531 ± 90	567[e]
biotinylated free duplex	12-bp duplex R5a, distal	23.0 ± 3.1	17.7 ± 2.4	1.32 ± 0.28	1.88 ± 0.31	79.1 ± 5.6	61.0 ± 4.4	390 ± 69	432 ± 68
	12-bp duplex R5a, central	26.0 ± 4.0	22.2 ± 3.1	1.07 ± 0.30	1.39 ± 0.29	82.7 ± 8.1	70.2 ± 5.0	337 ± 66	367 ± 64
	12-bp duplex R5a, proximal	21.0 ± 2.5	16.2 ± 1.9	1.51 ± 0.25	2.08 ± 0.28	69.9 ± 4.7	53.9 ± 3.4	396 ± 58	434 ± 58
Biotinylated bound to streptavidin	12-bp duplex R5a, distal	11.2 ± 1.0	8.95 ± 0.80	–	–	76.2 ± 4.3	60.8 ± 3.0	955 ± 86	991 ± 85
	12-bp duplex R5a, central	13.5 ± 1.2	11.48 ± 0.95	–	–	91.1 ± 4.5	77.3 ± 3.3	911 ± 81	943 ± 81
	12-bp duplex R5a, proximal	3.23 ± 0.34	2.61 ± 0.27	–	–	50.9 ± 4.4	41.1 ± 3.1	2520 ± 170	2540 ± 170

[a] The terms “central,” “distal,” and “proximal” refer to the three different spin label positions, as shown in Fig. 3(a). DNA sequences and nitroxide probe structures are shown in Fig. 1.

[b] Because this data does not employ the heating correction, we reference against a $\tau_{FFHS,bulk}$ value of 33.3 ps[10].

[c] The heating correction outlined previously[10], accounts for recent developments in ODNP and allows us to report more accurate measurements of ξ and $\tau_{FFHS}/\tau_{FFHS,bulk}$. Specifically, measurements of NMR $T_1(p)$ relaxation time as a function of microwave power, p, characterize the moderate effects of microwave heating on the ODNP enhancement and allow us to extract a more accurate value for k_σ and, in turn, $\xi(k_\sigma/k_{low})$. We reference corrected τ_{FFHS} measurements on DNA samples against the corrected measurement of $\tau_{FFHS,bulk}$ = 54.1 ps, which represents a more accurate value for the translational correlation time for free spin label in bulk water[10]. Thus, while we find that the ξ values are lower than estimated without the heating correction, the values of $\tau_{FFHS}/\tau_{FFHS,bulk}$ are, in fact, somewhat smaller – *i.e.*, correspond to faster dynamics. This correction proves to be especially relevant for the data presented here, since the values of τ_{FFHS} for DNA lie very close to the values of $\tau_{FFHS,bulk}$. Also note that though the values of k_ρ are the same for the corrected and uncorrected data, the resulting values of k_{low}, which are calculated from Eq. (S8), are different, as the values of k_σ are different.

[d] For all measurements, the standard deviation of the measurements was compared against an error estimate based on an estimate of the error in the raw data and the propagation of uncertainty. The greater of these two values was selected to represent the error.

[e] Since the initial set of experiments were acquired without the data needed to perform a heating correction, we estimate the heating-corrected values based on the fact that – for the later data – the heating correction tends to lower both ξ and k_σ by approximately 20%.